Radiation from relativistic jets in turbulent magnetic fields

K.-I. Nishikawa[*], M. Medvedev[†], B. Zhang[**], P. Hardee[‡], J. Niemiec[§], Å. Nordlund[¶], J. Frederiksen[¶], Y. Mizuno[*], H. Sol[‖] and G. J. Fishman[††]

[*]*National Space Science and Technology Center, Huntsville, AL 35805, USA*
[†]*Department of Physics and Astronomy, University of Kansas, KS 66045, USA*
[**]*Department of Physics, University of Nevada, Las Vegas, NV 89154, USA*
[‡]*Department of Physics and Astronomy, The University of Alabama, Tuscaloosa, AL 35487, USA*
[§]*Institute of Nuclear Physics PAN, ul. Radzikowskiego 152, 31-342 Kraków, Poland*
[¶]*Niels Bohr Institute, University of Copenhagen, Juliane Maries Vej 30, 2100 Copenhagen Ø, Denmark*
[‖]*LUTH, Observatore de Paris-Meudon, 5 place Jules Jansen, 92195 Meudon Cedex, France*
[††]*NASA/MSFC, Huntsville, AL 35805, USA*

Abstract. Using our new 3-D relativistic electromagnetic particle (REMP) code parallelized with MPI, we have investigated long-term particle acceleration associated with an relativistic electron-positron jet propagating in an unmagnetized ambient electron-positron plasma. The simulations have been performed using a much longer simulation system than our previous simulations in order to investigate the full nonlinear stage of the Weibel instability and its particle acceleration mechanism. Cold jet electrons are thermalized and ambient electrons are accelerated in the resulting shocks. The acceleration of ambient electrons leads to a maximum ambient electron density three times larger than the original value. Behind the bow shock in the jet shock strong electromagnetic fields are generated. These fields may lead to the afterglow emission. We have calculated the time evolution of the spectrum from two electrons propagating in a uniform parallel magnetic field to verify the technique.

Keywords: Weibel instability, magnetic field generation, synchrotron radiation
PACS: 98.70.Rz gamma-ray sources; gamma-ray bursts

RPIC SIMULATIONS

Particle-in-cell (PIC) simulations can shed light on the physical mechanism of particle acceleration that occurs in the complicated dynamics within relativistic shocks. Recent PIC simulations of relativistic electron-ion and electron-positron jets injected into an ambient plasma show that acceleration occurs within the downstream jet [1, 2, 3, 4, 5]. In general, these simulations have confirmed that relativistic jets excite the Weibel instability. The Weibel instability generates current filaments and associated magnetic fields [7], and accelerates electrons [1, 2, 3, 4, 5].

Pair Jets Injected into Unmagnetized Pair Plasmas using a Large System

We have performed simulations using a system with $(L_x, L_y, L_z) = (4005\Delta, 105\Delta, 105\Delta)$ and a total of ~ 1 billion particles (12 particles/cell/species for the ambient plasma) in the active grid zones [8]. In the simulations the electron skin depth, $\lambda_{ce} = c/\omega_{pe} = 10.0\Delta$, where $\omega_{pe} = (4\pi e^2 n_e/m_e)^{1/2}$ is the electron plasma frequency and the electron Debye length λ_e is half of the grid size. Here the computational domain is six times longer than in our previous simulations [4, 5]. The electron number density of the jet is $0.676n_e$, where n_e is the ambient electron density and $\gamma = 15$. The electron/positron thermal velocity of the jet is $v^e_{j,th} = 0.014c$, where $c = 1$ is the speed of light. Jets are injected in a plane across the computational grid at $x = 25\Delta$ in the positive x direction in order to eliminate effects associated with the boundary conditions at $x = x_{min}$. Radiating boundary conditions were used on the planes at $x = x_{min}$ & x_{max}. Periodic boundary conditions were used on all transverse boundaries. The ambient and jet electron-positron plasma has mass ratio $m_{e^-}/m_{e^+} = 1$. The electron/positron thermal velocity in the ambient plasma is $v^e_{a,th} = 0.05c$.

Figure 1 shows the averaged (in the $y-z$ plane) electron density and electromagnetic field energy along the jet at $t = 2000\omega_{pe}^{-1}$ and $3750\omega_{pe}^{-1}$. The resulting profiles of jet (red), ambient (blue), and total (black) electron density are shown in Fig. 1a. The ambient electrons are accelerated by the jet electrons and pile up towards the front part of jet. At the earlier time the ambient plasma density increases linearly behind the jet front as shown by the dashed blue line in Fig. 1a. At the later time the ambient plasma shows a rapid increase to a plateau behind the jet front, with additional increase to a higher plateau farther behind the jet front. The jet density remains approximately constant except near the jet front.

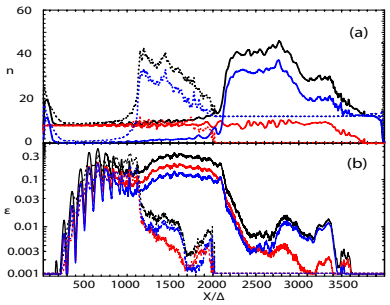

FIGURE 1. The averaged values of electron density (a) and field energy (b) along the x at $t = 3750\omega_{pe}^{-1}$ (solid lines) and $2000\omega_{pe}^{-1}$ (dashed lines). Fig. 1a shows jet electrons (red), ambient electrons (blue), and the total electron density (black). Fig. 1b shows electric field energy (blue), magnetic field energy (red), and the total field energy (black) divided by the total kinetic energy.

The Weibel instability remains excited by continuously injected jet particles and the electromagnetic fields are kept at a high level, about four times that seen in a previous much shorter grid simulation system ($L_x = 640\Delta$). At the earlier simulation time ($t = 2000\omega_{pe}^{-1}$) a large electromagnetic oscillating structure is generated and accelerates the ambient plasma. As shown in Fig. 1b, at the later simulation time the oscillating structure extends up to $x/\Delta = 1100$, then becomes more uniform and the magnetic field energy becomes larger than the electric field energy. These strong electromagnetic fields become very small beyond $x/\Delta = 2000$ in the shocked ambient region [4, 5].

The acceleration of ambient electrons becomes visible when jet electrons pass about $x/\Delta = 500$. The maximum density of accelerated ambient electrons is attained at $t = 1750\omega_{pe}^{-1}$. The maximum density gradually reaches a plateau as seen in Fig. 1a. The maximum electromagnetic field energy is located at $x/\Delta = 700$ as shown in Fig. 1b. The location of this maximum remains in this region at large simulation times.

New Numerical Method of Calculating Synchrotron and Jitter Emission from Electron Trajectories in Self-consistently Generated Magnetic Fields

Let a particle be at position $\mathbf{r_0}(t)$ at time t [6, 9]. At the same time, we observe the electric field from the particle from position $\mathbf{r}$. However, because of the finite propagation velocity of light, we observe the particle at an earlier position $\mathbf{r_0}(t')$ where it was at the retarded time $t' = t - \delta t' = t - \mathbf{R}(t')/c$. Here $\mathbf{R}(t') = |\mathbf{r} - \mathbf{r_0}(t')|$ is the distance from the charge (at the retarded time t') to the observer.

After some calculation and simplifying assumptions the total energy W radiated per unit solid angle per unit frequency from a charged particle moving with instantaneous velocity $\boldsymbol{\beta}$ under acceleration $\dot{\boldsymbol{\beta}}$ can be expressed as

$$\frac{d^2W}{d\Omega d\omega} = \frac{\mu_0 c q^2}{16\pi^3}\left|\int_{\infty}^{\infty}\frac{\mathbf{n}\times[(\mathbf{n}-\boldsymbol{\beta})\times\dot{\boldsymbol{\beta}}]}{(1-\boldsymbol{\beta}\cdot\mathbf{n})^2}e^{i\omega(t'-\mathbf{n}\cdot\mathbf{r_0}(t')/c)}dt'\right|^2 \quad (1)$$

Here, $\mathbf{n} \equiv \mathbf{R}(t')/|\mathbf{R}(t')|$ is a unit vector that points from the particle's retarded position towards the observer. The choice of unit vector $\mathbf{n}$ along the direction of propagation of the jet (hereafter taken to be the x-axis) corresponds to head-on emission. For any other choice of $\mathbf{n}$ (e.g., $\theta = 1/\gamma$), off-axis emission is seen by the observer. The observer's viewing angle is set by the choice of $\mathbf{n}$ ($n_x^2 + n_y^2 + n_z^2 = 1$).

In order to calculate radiation from relativistic jets propagating along the x direction [6] we consider a test case which includes a parallel magnetic field (B_x), and jet velocity of $v_{j1,2} = 0.99c$. Two electrons are injected with different perpendicular velocities ($v_{\perp 1} = 0.1c, v_{\perp 2} = 0.12c$). A maximum Lorenz factor of $\gamma_{max} = \{(1-(v_{j2}^2 + v_{\perp 2}^2)/c^2\}^{-1/2} = 13.48$ accompanies the larger perpendicular velocity.

Figure 2 shows electron trajectories in the $x-y$ plane (a: left panel), the radiation (retarded) electric field (red: $v_{\perp 1} = 0.12c$, blue: $v_{\perp 1} = 0.1c$) (b: middle panel), and spectra (right panel) for the case $B_x = 3.70$. The two electrons are propagating left to right with gyration in the $y-z$ plane (not shown). The gyroradius is about 0.44Δ for the electron with the larger perpendicular velocity. The power spectra were calculated at the point $(x,y,z) = (64,000,000\Delta, 43.0\Delta, 43.0\Delta)$. The seven curves show the power spectrum at viewing angles of 0° (red), 10° (orange), 20° (yellow), 30° (moss green), 45° (green), 70° (light blue), and 90° (blue). The higher frequencies become stronger at the 10° viewing angle . The critical angle for off-axis radiation $\theta_\gamma = \gamma_{max}^{-1}$ for this case is 13.48°. As shown in this panel, the spectrum at a larger viewing angle ($> 20^\circ$) has smaller amplitude.

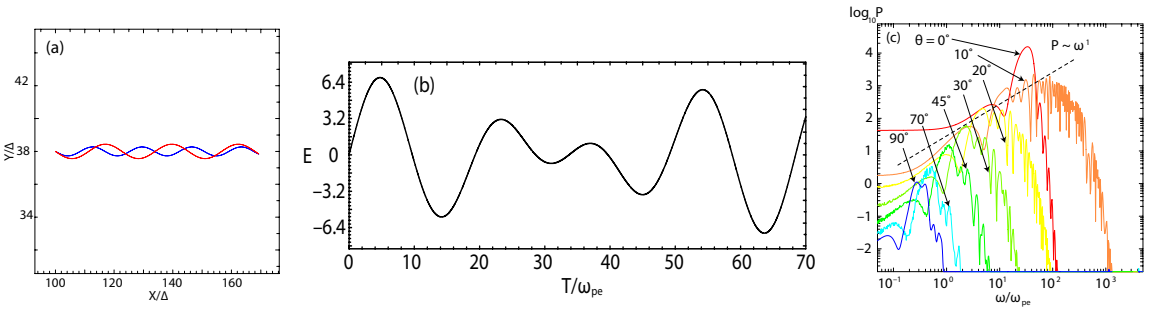

FIGURE 2. The paths of two electrons moving helically along the $x-$direction in a homogenous magnetic (B_x) field shown in the $x-y$-plane (a). The two electrons radiate a time dependent electric field. An observer situated at great distance along the n-vector sees the retarded electric field from the moving electrons (b). The observed power spectrum at different viewing angles from the two electrons (c). Frequency is in units of ω_{pe}^{-1}.

Since the jet plasma has a large velocity x-component in the simulation frame, the radiation from the particles (electrons and positrons) is heavily beamed along the x-axis (jitter radiation) [11].

In order to obtain the spectrum of synchrotron (jitter) emission, we consider an ensemble of electrons selected in the region where the Weibel instability has grown fully and electrons are accelerated in the generated magnetic fields. We will calculate emission from about 20,000 electrons during the sampling time $t_s = t_2 - t_1$ with Nyquist frequency $\omega_N = 1/2\Delta t$ where Δt is the simulation time step and the frequency resolution $\Delta\omega = 1/t_s$.

Emission obtained with the method described above is self-consistent, and automatically accounts for magnetic field structures on the small scales responsible for jitter emission. By performing such calculations for simulations with different parameters, we can investigate and compare the quite different regimes of jitter- and synchrotron-type emission [11]. The feasibility of this approach has already been demonstrated [9, 10], and its implementation is straightforward. Thus, we should be able to address the low frequency GRB spectral index violation of the synchrotron spectrum line of death [11].

ACKNOWLEDGMENTS

This work is supported by AST-0506719, AST-0506666, NASA-NNG05GK73G, NNX07AJ88G, NNX08AG83G, NNX08AL39G, and NNX09AD16G. JN was supported by MNiSW research projects 1 P03D 003 29 and N N203 393034, and The Foundation for Polish Science through the HOMING program, which is supported through the EEA Financial Mechanism.Simulations were performed at the Columbia facility at the NASA Advanced Supercomputing (NAS). and IBM p690 (Copper) at the National Center for Supercomputing Applications (NCSA) which is supported by the NSF. Part of this work was done while K.-I. N. was visiting the Niels Bohr Institute. Support from the Danish Natural Science Research Council is gratefully acknowledged.

REFERENCES

1. K.-I. Nishikawa, P. Hardee, G. Richardson, R. Preece, H. Sol, H., and G. J. Fishman, *ApJ*, **595**, 555–563 (2003)
2. K.-I. Nishikawa, P. Hardee, G. Richardson, R. Preece, H. Sol, H., and G. J. Fishman, *ApJ*, **623**, 927–937 (2005)
3. C. B. Hededal, and K.-I. Nishikawa, 2005, *ApJ*, **623**, L89–L92, (2005)
4. K.-I. Nishikawa, P. Hardee, C. B. Hededal, and G. J. Fishman, *ApJ*, **642**, 1267–1274 (2006)
5. E. Ramirez-Ruiz, K.-I. Nishikawa, and C. B. Hededal, *ApJ*, **671**, 1877–1885 (2007)
6. K.-I. Nishikawa, J. Niemiec, H. Sol, M. Medvedev, et al. in Proceedings of The 4th Heidelberg International Symposium on High Energy Gamma-Ray Astronomy, July 7-11, 2008, in Heidelberg, Germany (2008) (arXiv:0809.5067)
7. M. V. Medvedev, and A. Loeb, *ApJ*, **526**, 697–706 (1999)
8. K.-I. Nishikawa, J. Niemiec, M. Medvedev, H. Sol, P. E. Hardee, Y. Mizuno, B. Zhang, M. Pohl, and M. Oka, *ApJ*, in preparation (2008)
9. C.B. Hededal, Ph.D. thesis (2005) (arXiv:astro-ph/0506559)
10. C.B. Hededal, and Å. Nordlund, *ApJL*, submitted (2005) (arXiv:astro-ph/0511662)
11. M. V. Medvedev, *ApJ*, **637** 869–872 (2006)